Supplemental Material

Exploring complex mixtures by cyclic ion mobility high-resolution mass spectrometry – Application towards Petroleum

Christopher P. Rüger[1,2,3], Johann Le Maître[2,4], Julien Maillard[2,6], Eleanor Riches[5], Martin Palmer[5], Carlos Afonso[2,6], Pierre Giusti[2,4]

1 –Joint Mass Spectrometry Centre (JMSC)/Chair of Analytical Chemistry, University of Rostock, 18059 Rostock, Germany

2 – International Joint Laboratory–iC2MC: Complex Matrices Molecular Characterization, Total Research and Technology Gonfreville (TRTG), 76700 Harfleur, France

3 – Department Life, Light & Matter (LLM), University of Rostock, 18051 Rostock, Germany

4 – TOTAL Refining and Chemicals, Gonfreville, 76700 Harfleur, France

5 – Waters Corporation, SK9 4AX Wilmslow, United Kingdom

6 – Normandie Université, COBRA, UMR 6014 et FR 3038, Université de Rouen-Normandie, INSA de Rouen, CNRS, IRCOF, 76130 Mont Saint Aignan, France

* – corresponding author: carlos.afonso@univ-rouen.fr

Keywords

Cyclic ion mobility spectrometry, high-resolution mass spectrometry, petroleum, complex mixtures, electrospray ionization, atmospheric pressure photoionization

Table of Content

observed. The drift times of the separated isobaric distributions are comparable between the samples allowing us to hypothesize similar structural groups in VGO A, B, and C.

Figure S6: Theoretical workflow for the combination of ion mobility and mass spectrometric resolving power for approaching narrow *m/z*-splits. Target peaks are initially identified based on the distorted FWHM (resolving power significantly lower than theoretically expected for the mass spectrometer platform).

Figure S7: Deconvoluted mass spectra based on the weighted average of the fitted Gaussian curves for VGO B and C according to the workflow presented in Figure S6 and shown in detail in Figure 5 of the main body. The *m/z*-difference between the apex peak position account for 3.0 and 3.4 mDa close to the exact split of C_3/SH_4 3.4 mDa.

Table S1: Short name and description of the different experimental types for the cIMS HRMS utilized in this study. Details of the instrumental setup are given in Scheme S1.

#	Name	Description
1	QcIMS	Quadrupole precursor selection with *m/z* 1-60 window width → cyclic ion mobility separation with optimized pass number → high-resolution time-of-flight mass spectrometric detection (see Scheme S2)
2	Slicing	QcIMS (#1) with 1 Da window and one pass → Ejection of a 1 ms section (slice) into the pre-array store and discarding the remaining ions in the cyclic region → Re-injection of the ions stored in the pre-array store into the cIMS and separation via additional passes → high-resolution time-of-flight mass spectrometric detection (see Scheme S3)
3	Core analysis	All-ion-fragmentation with a collision voltage of 75 V predominantly leading to dealkylation → Ion mobility spectra of a certain *m/z* range sliced and following the procedure of #2 with an optimized number of passes (see Scheme S4)

Please notice, a more detailed step-by-step description of the basic cyclic ion mobility spectrometry experiments can also be found elsewhere (1).

(1) Eldrid, C.; Ujma, J.; Kalfas, S.; Tomczyk, N.; Giles, K.; Morris, M.; Thalassinos, K., Gas Phase Stability of Protein Ions in a Cyclic Ion Mobility Spectrometry Traveling Wave Device. *Anal. Chem.* **2019**, *91* (12), 7554–7561, DOI: 10.1021/acs.analchem.8b05641.

Scheme S1: Schematic illustration of the instrumental setup of the cyclic ion mobility high-resolution time-of-flight mass spectrometer.

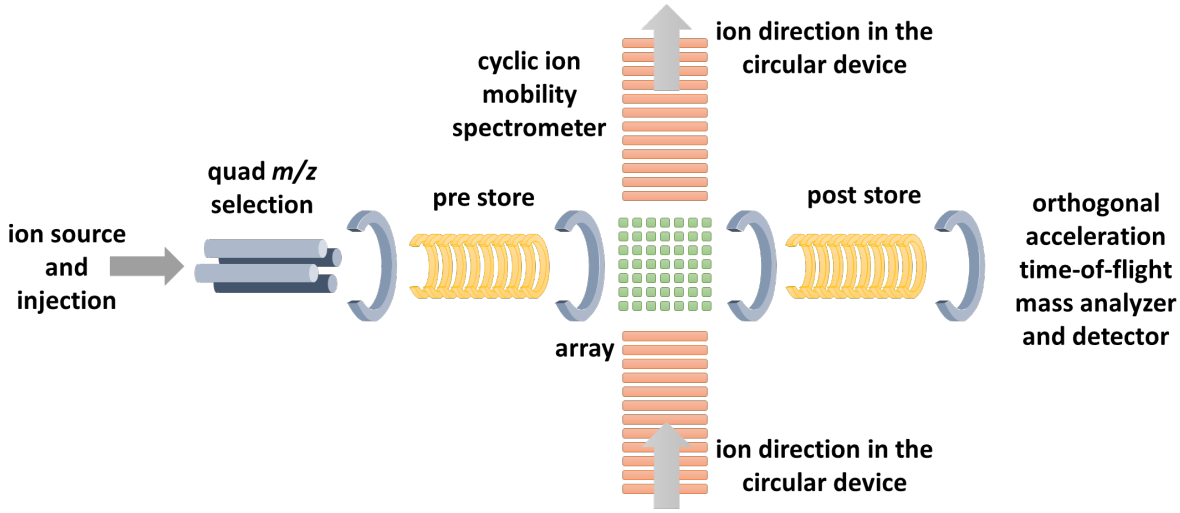

Scheme S2: Graphical description of the first experimental design (Table S1, 1) QcIMS with the different consecutive steps. More details on the instrumental setup are given in Scheme S1.

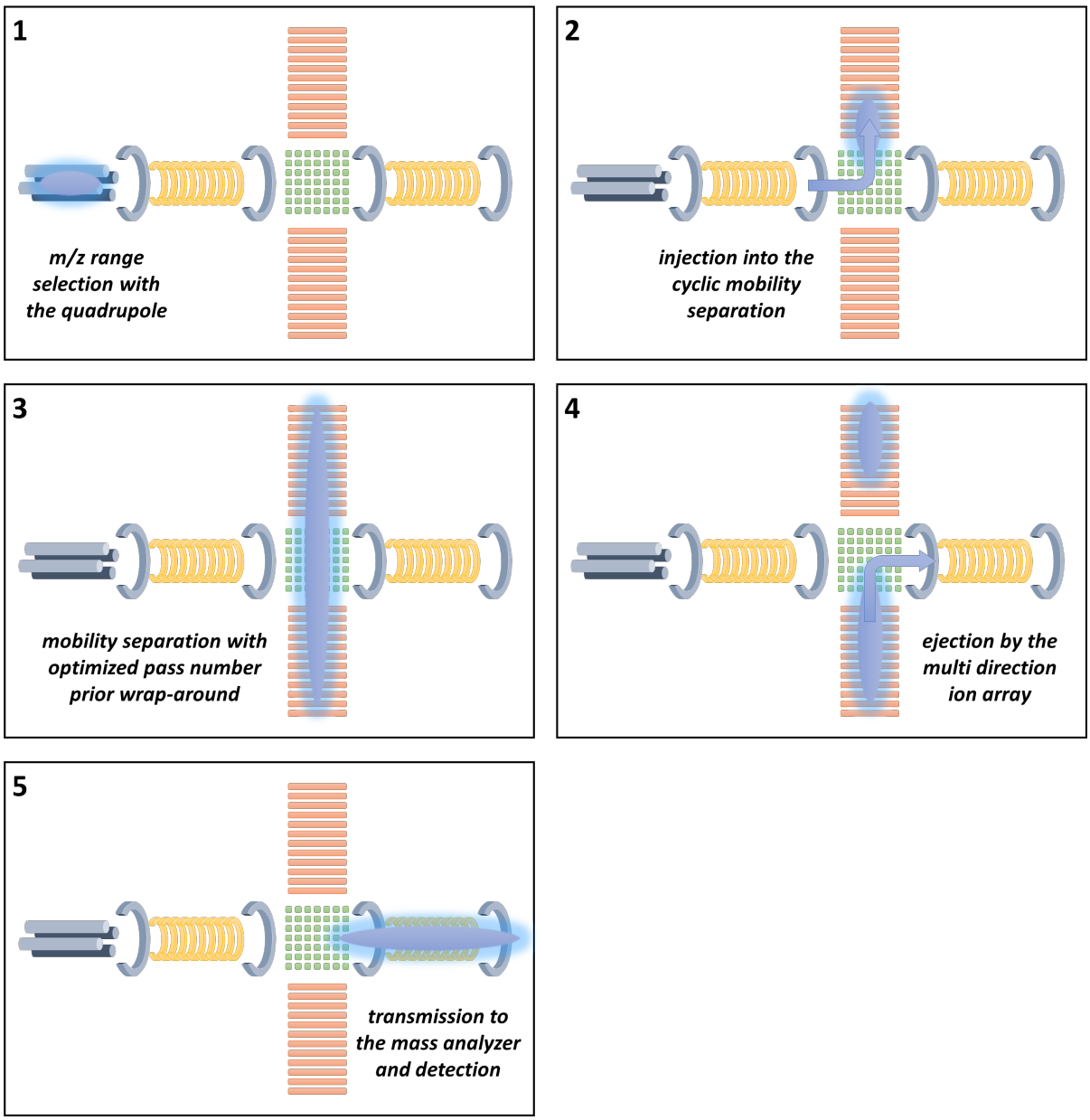

Scheme S3: Graphical description of the second experimental design (Table S1, 2) slicing with the different consecutive steps. More details on the instrumental setup are given in Scheme S1.

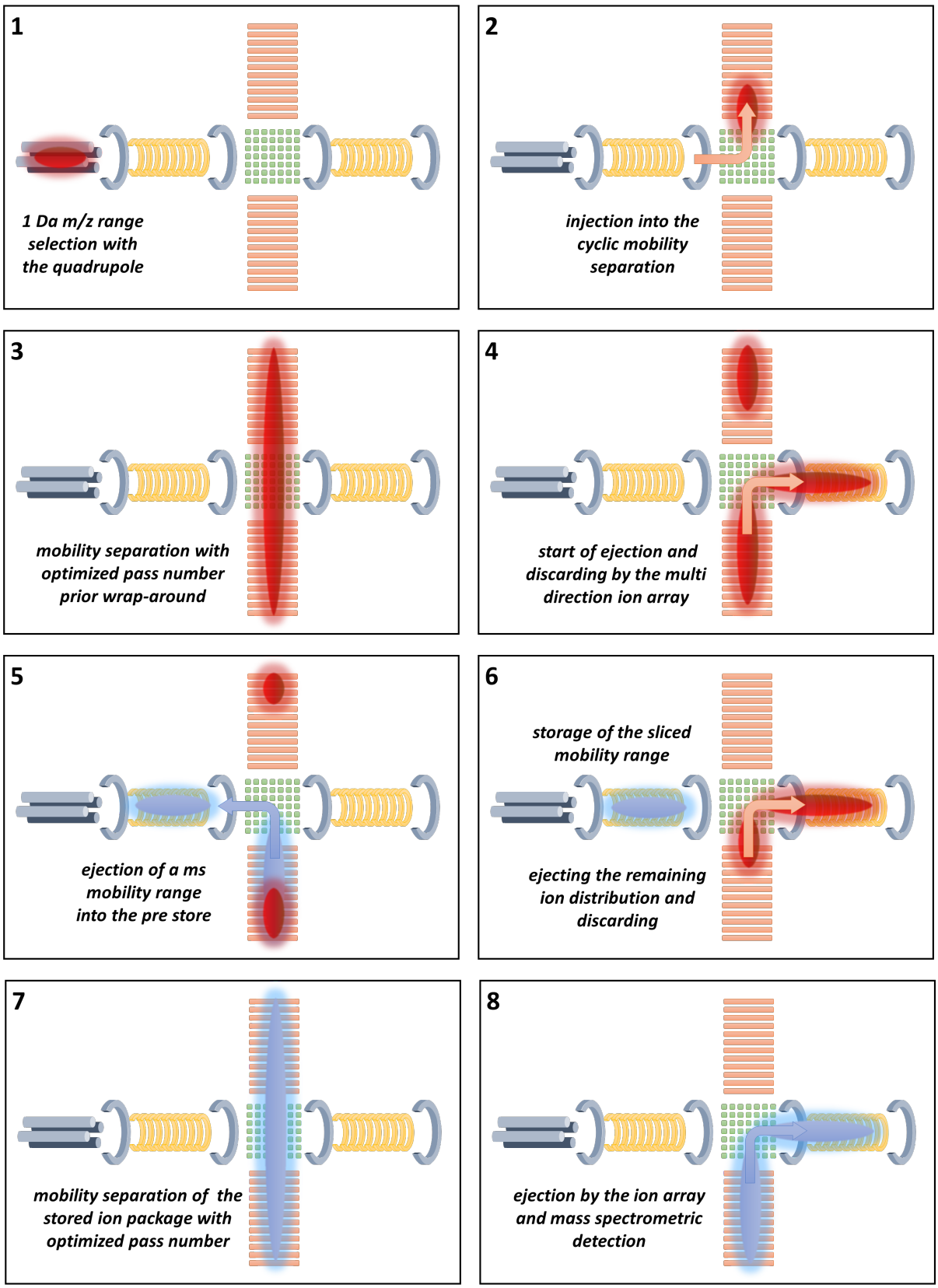

Scheme S4: Graphical description of the third experimental design (Table S1, 3) core analysis with the different consecutive steps. More details on the instrumental setup are given in Scheme S1. Two concepts after collision induced fragmentation are possible given in step 5a or 5b-7b.

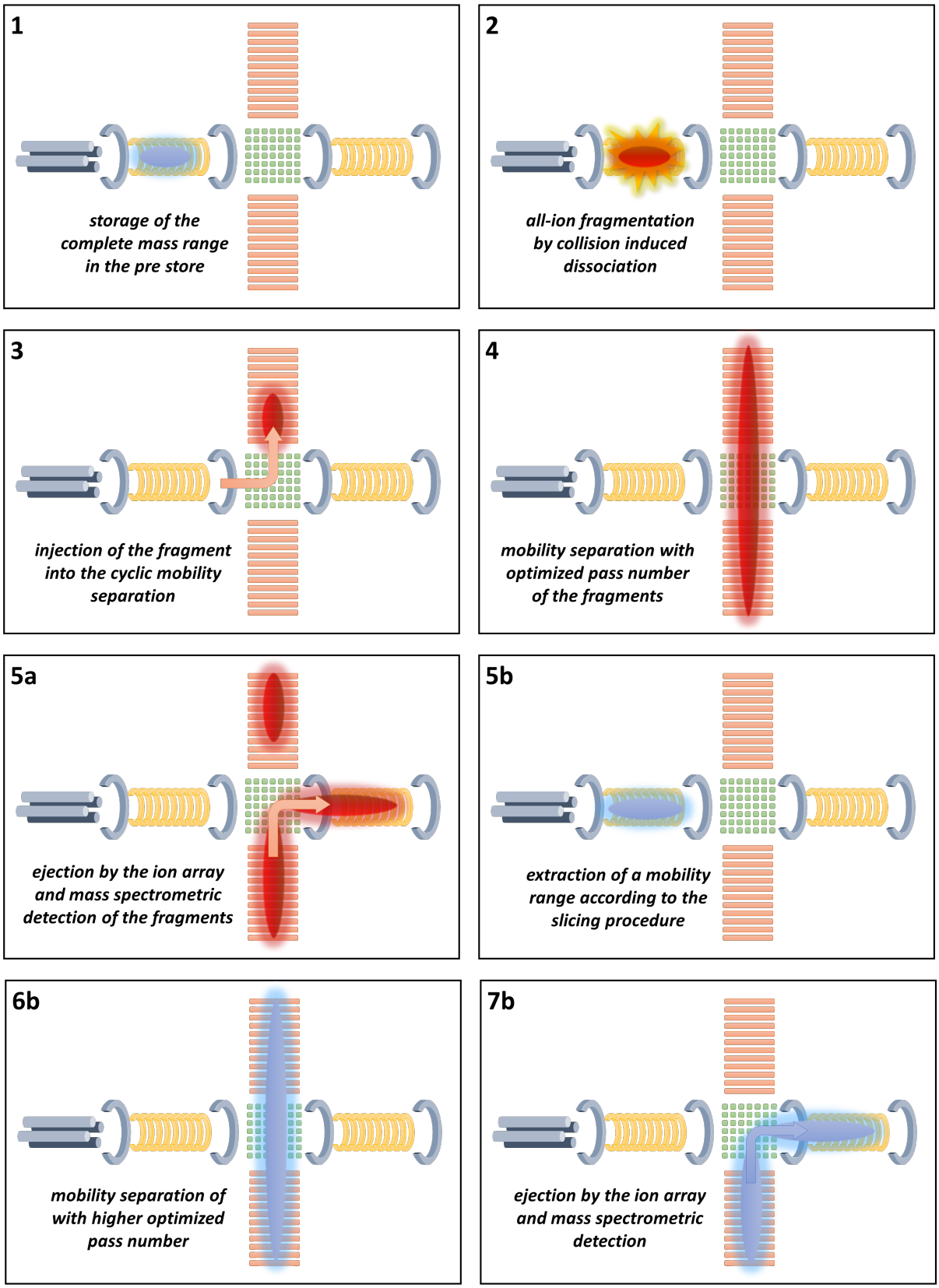

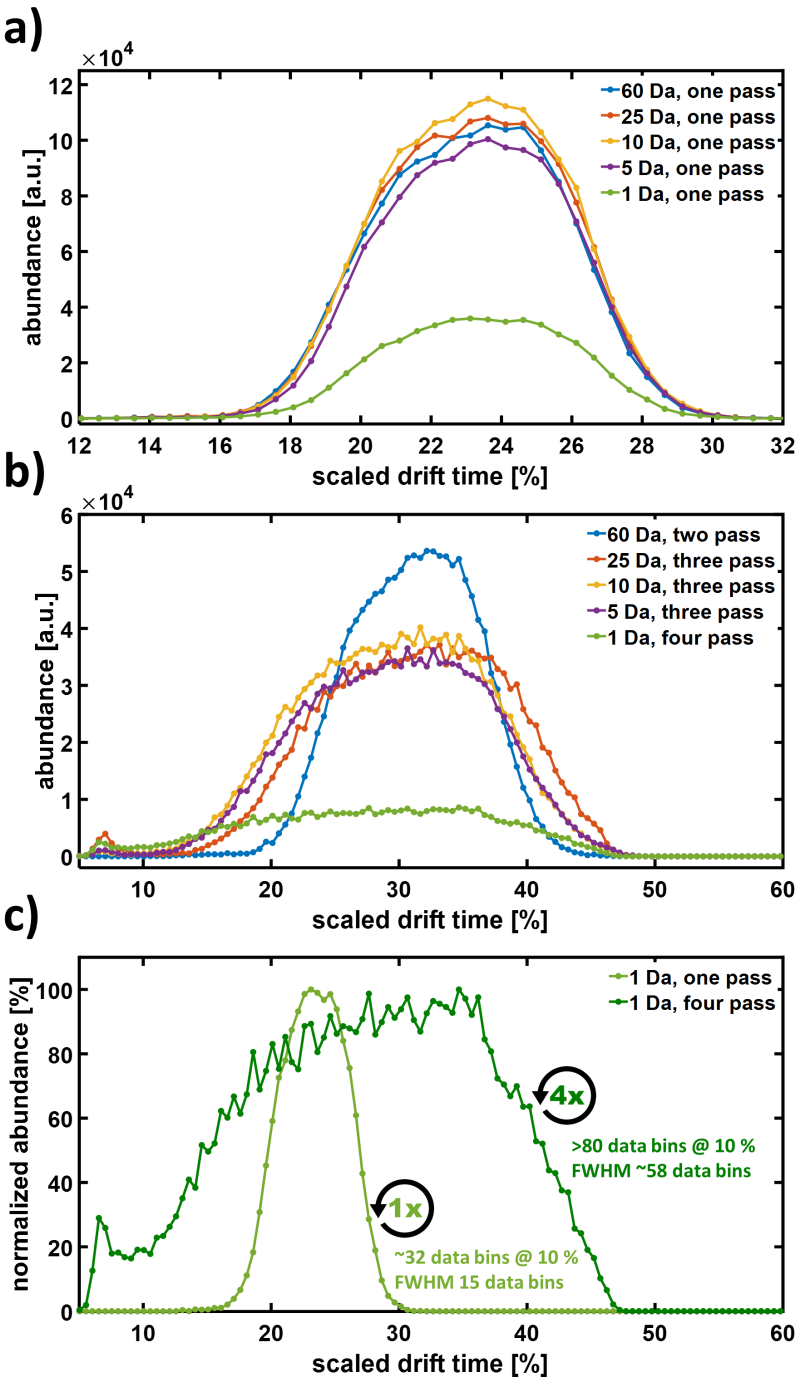

Figure S1: Positive-mode electrospray ionization of a vacuum gas oil, $C_{27}H_{40}N_1^+$ (DBE 9, ± 20 mDa) is depicted. a) Extracted ion mobility profile with one pass and various quadrupole isolation widths centered at *m/z* 378. b) Extracted ion mobility profile with the optimized pass number and various quadrupole isolation widths. c) Comparison of the data bins recorded over the arrival time distribution of a single Da isolation window between one and four passes. The improvement in peak description based on the number of data points along the signal (bins) can be depicted. Please note the scaled drift time allowing direct comparison between the different pass numbers.

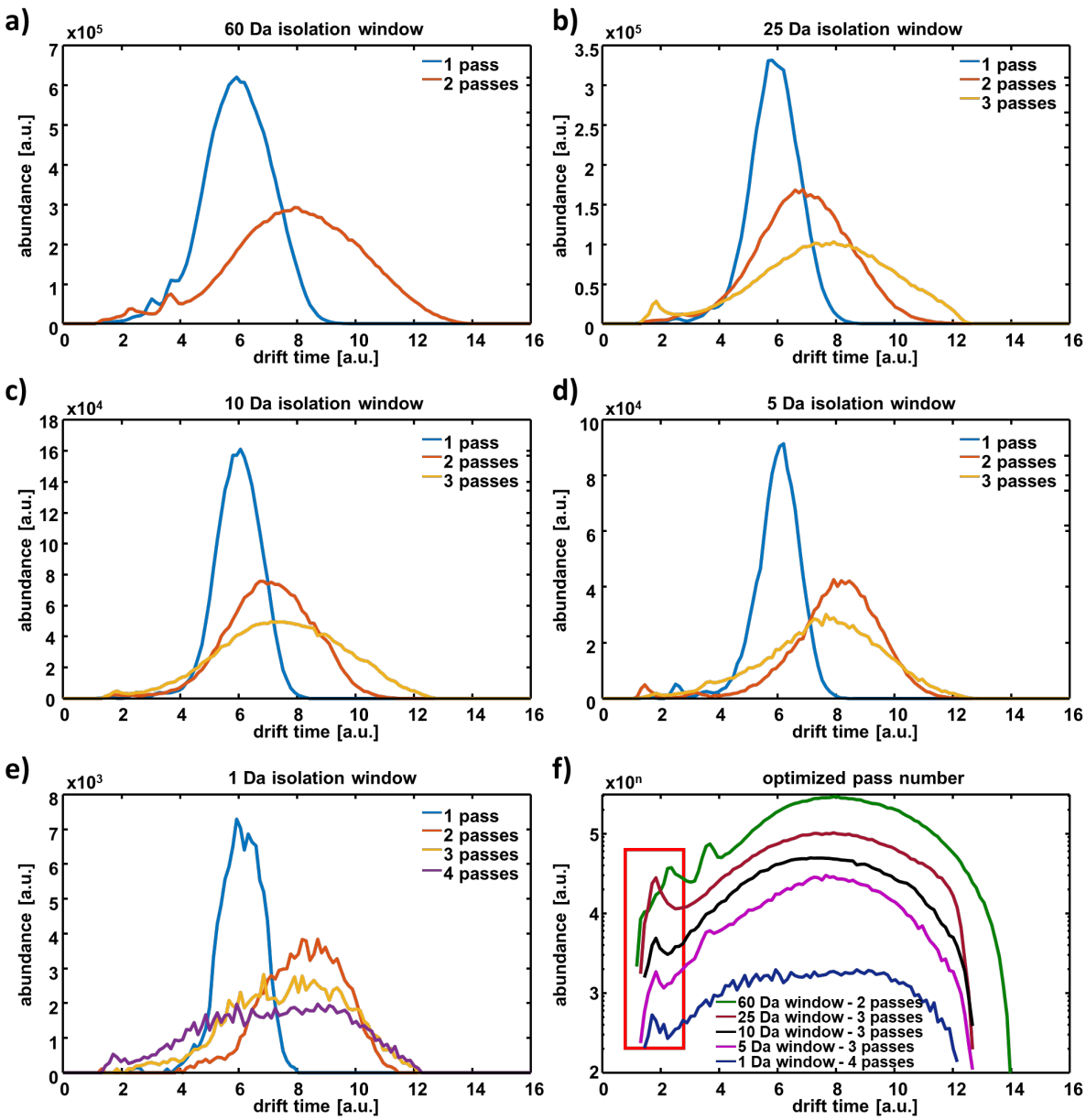

Figure S2: a)-e) Total ion count arrival time distribution for the stepwise decrease of the quadrupole isolation width from 60 to 1 Da centered at *m/z* 378 and increase of the number of passes prior occurring of the wrap-around effect. At very low isolation width, individual features, by means of spikes, can be depicted. f) The red square reveals a minor abundance of the wrap-around effect (sharp edge at the beginning of the distribution) utilizing the logarithmic scaling for visualization.

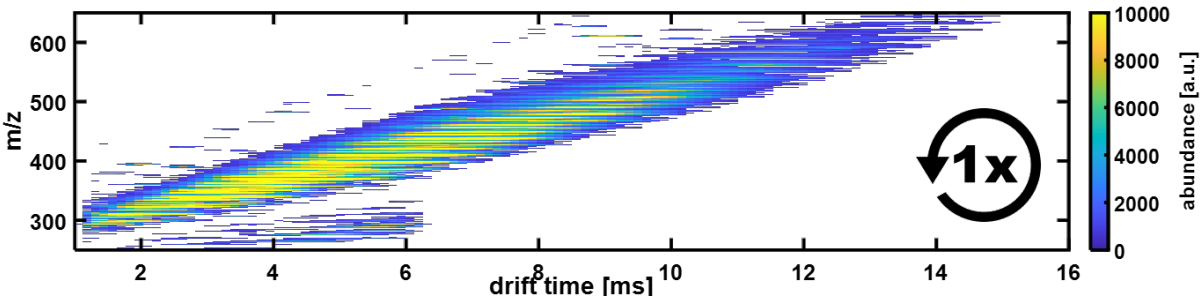

Figure S3: Broadband survey IMS-MS overview. Cyclic ion mobility spectrometry for one pass of a vacuum gas oil sample introduced by electrospray ionization.

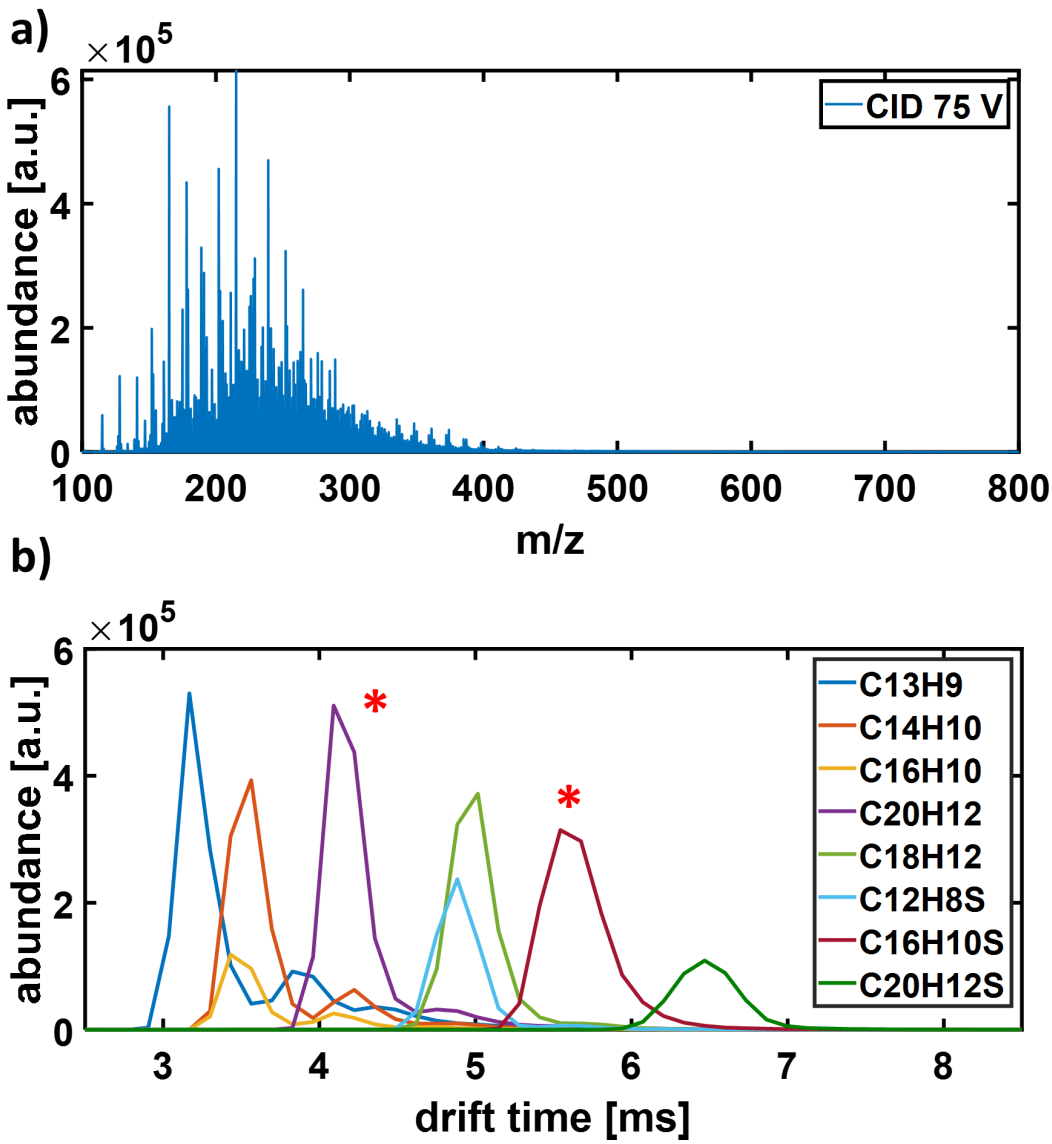

Figure S4: a) Average atmospheric pressure photo ionization mass spectrum for VGO A of the all-ion fragmentation deploying collision-induced dissociation at 75 V. b) Extracted ion mobility spectra for selected aromatic core structure targets (± 10 mDa). Asterisks indicate the two targets, $C_{20}H_{12}$ as a polycyclic aromatic hydrocarbon (PAH) and $C_{16}H_{10}S$ as a polycyclic aromatic sulfur heterocycle (PASH). Please note for simplicity reasons species given as parent molecule sum formula here.

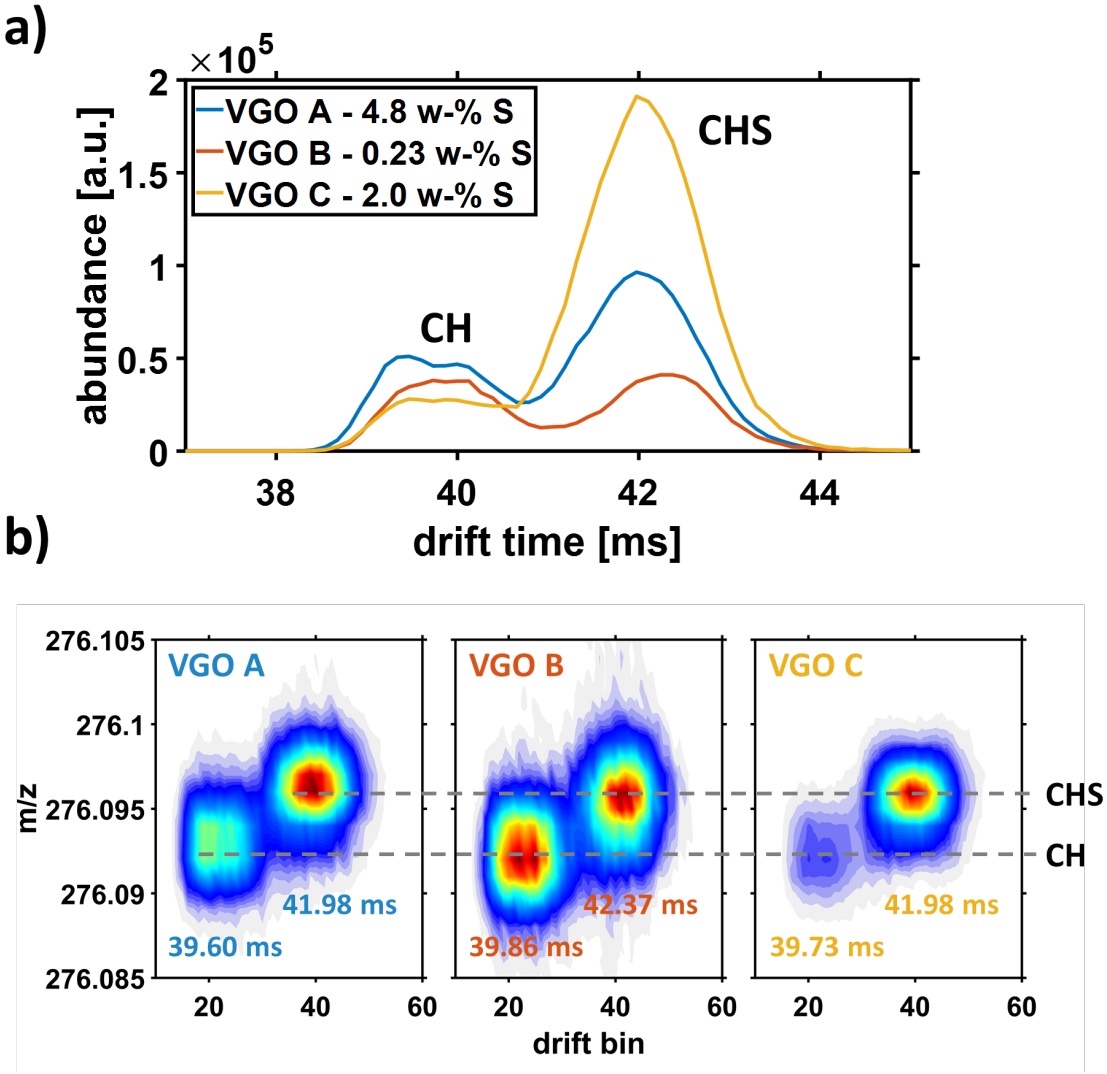

Figure S5: Atmospheric pressure photo ionization of VGO A, B, and C – NM 276 isolated with the quadrupole at 1 Da width. a) Arrival time distribution of the optimized pass number of three turns for the extracted arrival time distribution of *m/z* 276.09 – 276.10. b) Survey visualization of drift bins versus *m/z* of the three pass separation. The separation of the two isomeric distributions, attributed to the CH- and CHS-class isomers, can be clearly observed. The drift times of the separated isobaric distributions are comparable between the samples allowing us to hypothesize similar structural groups in VGO A, B, and C.

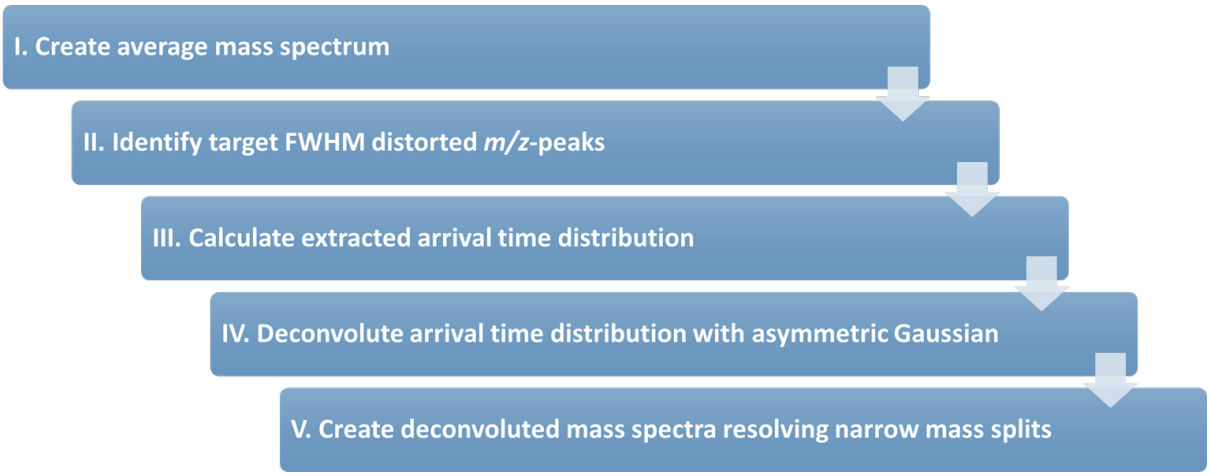

Figure S6: Theoretical workflow for the combination of ion mobility and mass spectrometric resolving power for approaching narrow *m/z*-splits. Target peaks are initially identified based on the distorted FWHM (resolving power significantly lower than theoretically expected for the mass spectrometer platform).

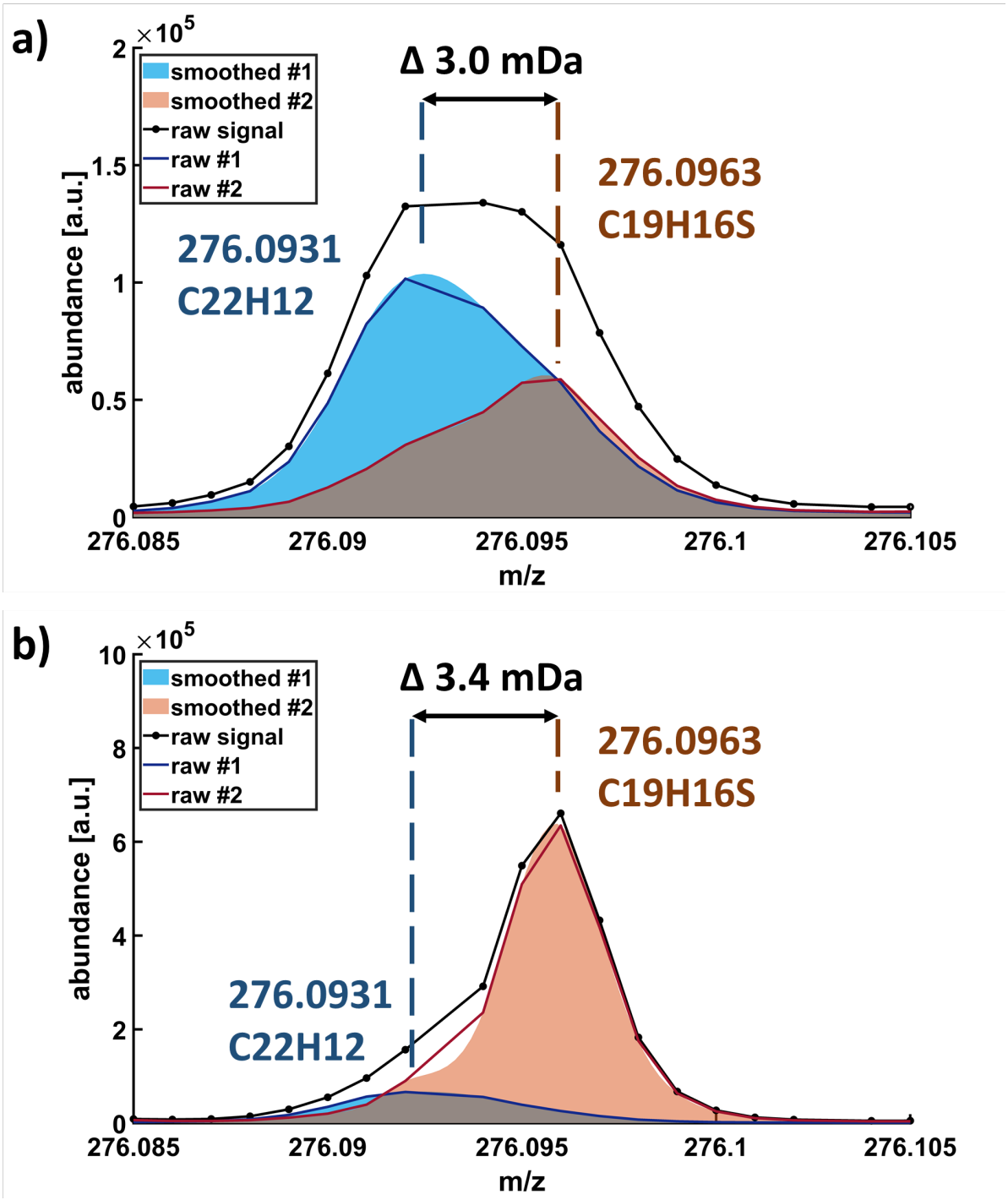

Figure S7: Deconvoluted mass spectra based on the weighted average of the fitted Gaussian curves for VGO B and C according to the workflow presented in Figure S6 and shown in detail in Figure 5 of the main body. The *m/z*-difference between the apex peak position account for 3.0 and 3.4 mDa close to the exact split of C_3/SH_4 3.4 mDa.